MATERIALS ENGINEERING

10.1126/sciadv.1600209

Subatomic deformation driven by vertical piezoelectricity from CdS ultrathin films

Xuewen Wang,[1,2]* Xuexia He,[1]* Hongfei Zhu,[3] Linfeng Sun,[4] Wei Fu,[1] Xingli Wang,[5] Lai Chee Hoong,[1] Hong Wang,[1] Qingsheng Zeng,[1] Wu Zhao,[1] Jun Wei,[6] Zhong Jin,[3] Zexiang Shen,[4] Jie Liu,[3,7] Ting Zhang,[2†] Zheng Liu[5,8,9†]

Driven by the development of high-performance piezoelectric materials, actuators become an important tool for positioning objects with high accuracy down to nanometer scale, and have been used for a wide variety of equipment, such as atomic force microscopy and scanning tunneling microscopy. However, positioning at the subatomic scale is still a great challenge. Ultrathin piezoelectric materials may pave the way to positioning an object with extreme precision. Using ultrathin CdS thin films, we demonstrate vertical piezoelectricity in atomic scale (three to five space lattices). With an in situ scanning Kelvin force microscopy and single and dual ac resonance tracking piezoelectric force microscopy, the vertical piezoelectric coefficient (d_{33}) up to 33 pm·V^{-1} was determined for the CdS ultrathin films. These findings shed light on the design of next-generation sensors and microelectromechanical devices.

INTRODUCTION

Piezoelectric material has proven to be a key to achieving high-resolution positioning, which is crucial for fundamental research and industrial applications. Recent studies on the piezoelectricity of two-dimensional (2D) materials provide opportunities for constructing thin electromechanical coupled devices, such as nanoscale mechanical transducers and microenergy systems (*1*–*3*). Because of the break of centrosymmetry in monolayer crystals, only a few 2D layered materials (including graphene, h-BN, C_3N_4, and 2H-ACh_2, where A = W, Mo; *Ch* = S, Se, Te) have been predicted to have piezoelectricity (*4*, *5*), which has been exemplified in a few layered MoS_2-based flexible and suspended devices (*1*, *2*, *6*). In these studies, in-plane strain was produced by an atomic force microscopy (AFM) tip (or flexible substrate) on the films, which resulted in charge aggregation when a lateral bias was applied to the materials (Fig. 1). However, these methods can only be used to study in-plane piezoelectricity, such as d_{11} and d_{22}, although the vertical piezoelectric coefficient (d_{33}) is the key parameter to evaluate the performance of piezoelectric materials.

For intrinsic piezoelectric materials, vertical symmetry breaking still remains even for thin films down to a few layers of atoms. Therefore, theoretically, the vertical piezoelectricity (d_{33}) can be obtained from ultrathin piezoelectric materials such as ZnO, CdS, and CdSe nanoplatelets. In this case, when the stress is applied to ultrathin piezoelectric materials toward out of plane, the geometric deformation will generate negative and positive charges simultaneously. These charges will distribute at the top and bottom surfaces under external bias (Fig. 1). However, the synthesis of ultrathin piezoelectric materials is the main challenge to determining the vertical piezoelectricity (d_{33}). Up to now, a few studies reported the synthesis of atomic thin piezoelectric materials (such as ZnO, CdS, and CdSe nanoplatelets), by a wet chemical method (*7*–*10*). Although these achievements present valuable advances, many critical problems still remain and limit their applications. For instance, because of organic solutions that were used to synthesize CdS, the remaining organic molecules at the surface of CdS may cast shadows on the piezoelectricity of CdS. Here, using chemical vapor deposition, we synthesized the CdS thin films down to 2 to 3 nm. We demonstrate the vertical piezoelectricity d_{33} of CdS in atomic scale (three to five space lattices) by single and dual ac resonance tracking piezoelectric force microscopy (DART-PFM). The surface potential and charge distribution were measured by scanning Kelvin force microscopy (SKFM). We observed the vertical piezoelectric domains at the CdS thin films, and the measured piezoelectric coefficient (d_{33}) was 32.8 pm·V^{-1}. We found that this value was approximately three times larger than that of the bulk CdS. In addition, we found that the contact PFM process could largely change the surface potential of a CdS thin film by producing the charges at its surface. This study sheds light on the vertical piezoelectricity of ultrathin (lattice scale) nanomaterials and promotes their application in actuators with subatomic resolution.

RESULTS AND DISCUSSION

Growth of CdS thin films for vertical piezoelectricity

We synthesized CdS thin films onto SiO_2/Si substrate by chemical vapor deposition with sulfur powder and Cd grains as precursors (see details in Materials and Methods and fig. S1A). Figure 2 shows three dominant morphologies of CdS thin films (i) uniform disc-like structures, (ii) Janus structure with two kinds of thickness at one thin film, and (iii) rounded microparticle at the center of a thin film. The typical optical microscopic images are shown in Fig. 2 (A, D, and G), and all the samples are circular. The radius of the as-prepared thin film is between 10 and 20 μm. To identify the thickness of as-prepared CdS thin films,

[1]School of Materials Science and Engineering, Nanyang Technological University, 50 Nanyang Avenue, Singapore 639798, Singapore. [2]International Laboratory for Adaptive Bio-nanotechnology (i-Lab), Suzhou Institute of Nano-Tech and Nano-Bionics, Chinese Academy of Sciences, Suzhou 215123, China. [3]Key Laboratory of Mesoscopic Chemistry of Ministry of Education and Collaborative Innovation Center of Chemistry for Life Sciences, School of Chemistry and Chemical Engineering, Nanjing University, Nanjing 210093, China. [4]School of Physical and Mathematical Sciences, Nanyang Technological University, 21 Nanyang Link, Singapore 637371, Singapore. [5]Centre for Micro-/Nano-electronics (NOVITAS), School of Electrical and Electronic Engineering, Nanyang Technological University, Singapore 639798, Singapore. [6]Singapore Institute of Manufacturing Technology, 71 Nanyang Drive, Singapore 638075, Singapore. [7]Department of Chemistry, Duke University, Durham, NC 27708, USA. [8]Center for Programmable Materials, School of Materials Science and Engineering, Nanyang Technological University, 50 Nanyang Avenue, Singapore 639798, Singapore. [9]CINTRA CNRS/NTU/THALES, UMI 3288, Research Techno Plaza, 50 Nanyang Drive, Singapore 637553, Singapore.
*These authors contributed equally to this work.
†Corresponding author. Email: z.liu@ntu.edu.sg (Z.L.); tzhang2009@sinano.ac.cn (T.Z.)

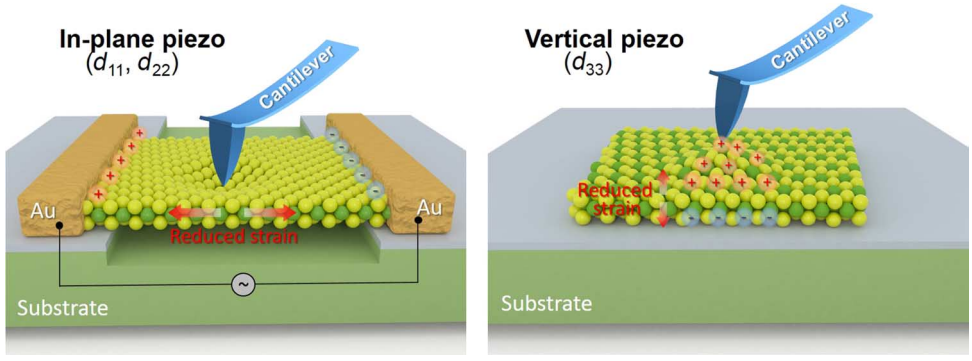

Fig. 1. Schematic illustration of local characterization of in-plane piezoelectricity and vertical piezoelectricity. In-plane piezoelectricity (piezo) (d_{11}, d_{22}) of ultrathin materials is the planar electromechanical couple behavior, where the applied stress and produced piezoelectric potential are located at the in-plane of exposed lattice plane. Vertical piezoelectricity (d_{33}) focus on electromechanical interaction occurred in the vertical axis, which is perpendicular to the surface of materials. The high-precision deformation actuator can be implemented using accurate positioning of the materials surface by vertical inverse piezoelectricity.

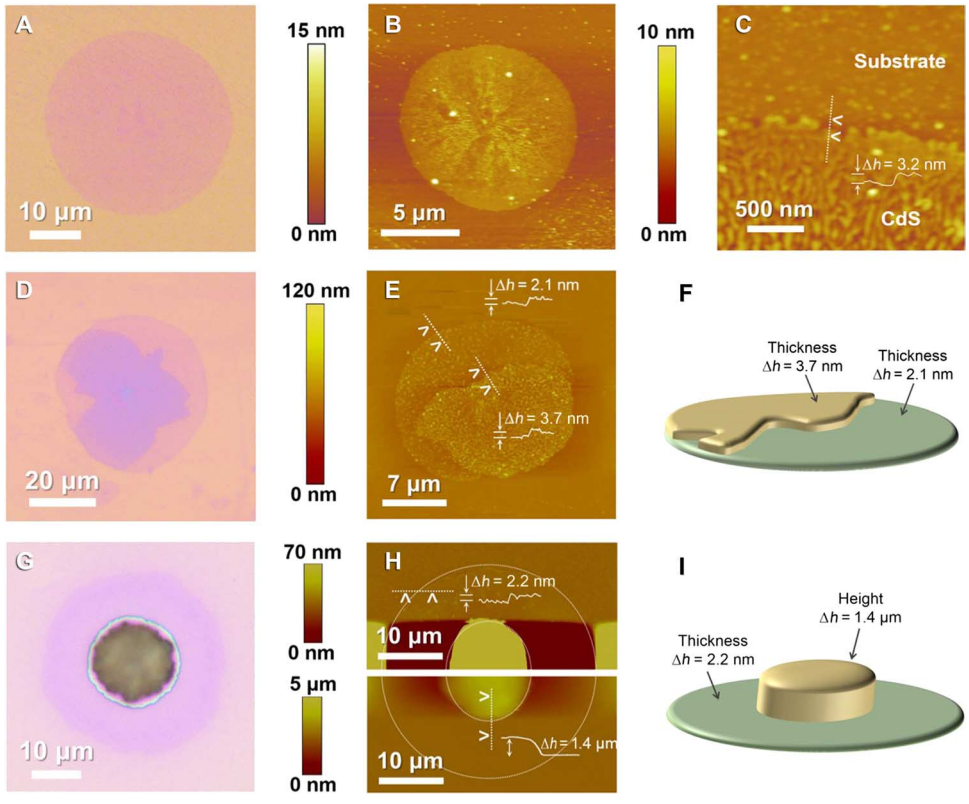

Fig. 2. CdS thin films with three different shapes. (**A** to **E**, **G**, and **H**) Typical optical images (A, D, and G) and AFM images (B, C, E, and H) of CdS thin films with uniform disc-like structure, Janus structure, and the structure of rounded microparticle at its center. The AFM line scan in (C) indicates that the thickness of the CdS ultrathin film is ~3.2 nm, corresponding to approximately five lattices of CdS. The AFM line scans in (E) and (H) show that the Janus structure has two kinds of thickness (2.1 and 3.7 nm) at one thin film, and the structure of the microparticle is grown on the thin film with a height (h) of ~1.4 μm and radius of ~5 μm. (**F** and **I**) Corresponding structural diagram.

we characterized the samples by AFM (Fig. 2, B, C, E, and H). The thickness of these thin films ranges from 2.1 to 3.7 nm, which is close to the thickness of three to five crystal lattices (2.02 nm for three lattices and 3.37 nm for five lattices) of hexagonal CdS along the z orientation. The Janus structure has different geometries at the thin film (Fig. 2F). For the third structure, circular microparticles were grown on the thin film (2.2 nm). The height and radius of the particles are ~1.4 and ~5 μm, respectively (Fig. 2I). We examined more than 100 CdS thin films to calculate their size distribution (fig. S2). The three types of thin films present average sizes of 8.92, 48.33, and 27.08 μm, respectively, with the Gaussian distribution. The SDs of the sizes are 0.84, 17.65, and 7.75 μm, respectively. The average size of the Janus structure is larger

than that of the uniform disc-like structures, which suggests that the secondary nucleation could be preferentially formed in a large thin film.

Spectroscopic characterization of CdS thin films

We collected Raman spectra from these materials and were able to identify the wurtzite CdS by the Raman vibration modes (*11*, *12*). The first- and second-order longitudinal optical phonons in CdS thin films were observed from Raman spectra (fig. S3), which matched the Raman spectra of nanowires (*12*–*14*). It is well known that the optical properties of nanomaterials show significant departures from their bulk counterparts, because the scale of confinement approaches their exciton Bohr radius (*15*). Notably, the thickness of our CdS thin films is in the range of 2 to 3 nm, which is close to the exciton Bohr radius of CdS (~3.1 nm) (*16*, *17*). To understand the optical properties of the as-prepared CdS thin film, we investigated their band gap structure and photoluminescence (PL). Figure 3A represents the energy band structure of CdS in the vicinity of the Γ-point of the Brillouin zone, showing the direct gap emission at Γ-valley (green arrow) as well as electron transitions between defect energy level and electron band (yellow arrow), which results in photoemission with band gap fluorescence and defect-related luminescence (*7*). The PL properties for all three kinds of CdS thin film were obtained at room temperature using 457-nm laser as an excitation source (Fig. 3, B to F, and fig. S4). Only a strong emission peak at ~506 nm was observed from the ultrathin CdS thin film with a thickness of 2 to 3 nm, which is considered to be band edge emission. Notably, the value is close to the band edge emission of bulk CdS (~514 nm) with a slight blue shift. Similar near–band edge emissions from CdS quantum dots, nanowires, and nanoribbons were also observed in previous reports (*7*, *18*, *19*). This phenomenon can be explained by quantum confinement effect in a 2D thin film. As the dimension of the materials reaches nanoscale (close to the exciton Bohr radius), the electrons and holes will be squeezed into a confining dimension, following the appearance of discrete energy states. Therefore, the band gap increases and becomes size-dependent, which ultimately gives rise to a blue shift in band edge emission (*15*, *20*). For the circular microparticle at the center of the thin film, the PL spectrum displays a pronounced peak at 595 nm other than band edge emission at 514 nm (Fig. 3B). This contributed to the defect-related emission from trap or surface states, for example the unreacted sulfur atoms at the interface and Cd vacancies.

We also collected the PL spectra and PL mapping from different types of CdS thin films (Fig. 2, D to F, and fig. S4). Figure 3C shows the typical optical microscopic image of the rounded microparticles at the center of the thin film and the corresponding PL intensity mapping at a peak of 514 nm. Different scale bars were applied to Fig. 3 (D and E) to reflect the fine structure of the CdS thin films. The PL mapping at the outside area suggests a high uniformity and homogeneity of CdS thin films. Meanwhile, strong and ring-like PL emission was observed at the middle range of the sample. The intensity of PL emission from the microparticle is much stronger than that from the thin film. Therefore, it is difficult to recognize the small distinction of PL mappings between those two materials, despite the fact that there is ~8-nm disparity for band edge emissions at different positions. The intensity of PL mapping at 595 nm confirms that the defect-related emission only existed at the

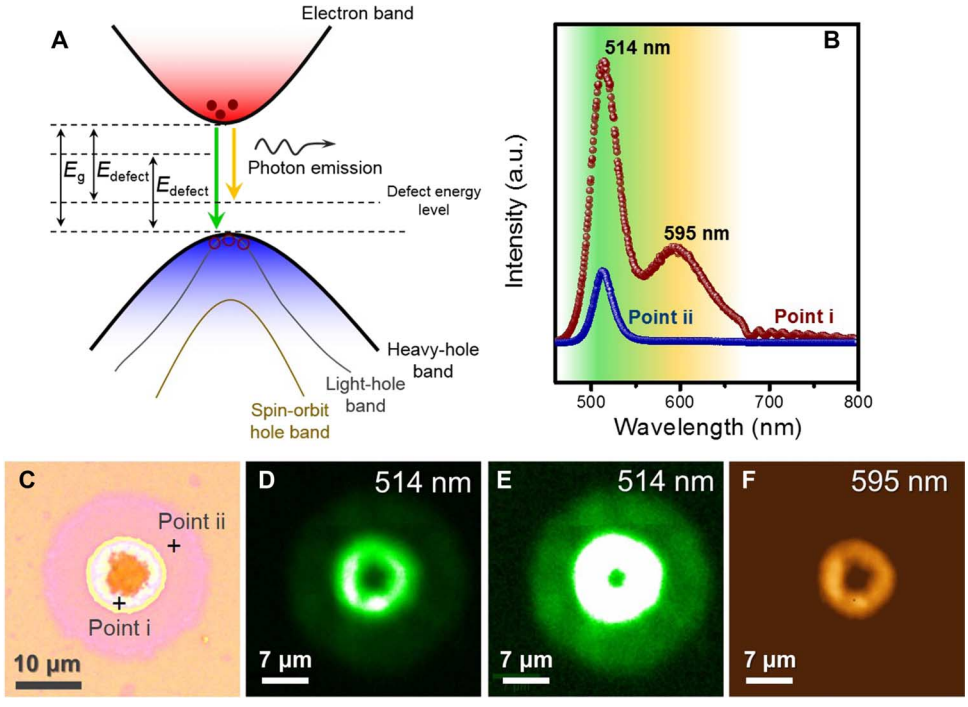

Fig. 3. Spectroscopic characterization of CdS thin film. (**A**) Energy (*E*) band structure in the vicinity of the Γ-point of the Brillouin zone, showing the photon emission process. (**B** and **C**) PL spectrum of CdS thin film from points i and ii marked in (C) with plus signs, showing strong band edge emission (506 nm) of CdS ultrathin film and defect-related emission (595 nm). (C) Optical image of CdS thin film with a rounded microparticle at its center. a.u., arbitrary units. (**D** and **E**) PL mapping at an emission of 514 nm with a different scale bar, demonstrating high uniformity and homogeneity of CdS thin films at the outside area. (**F**) PL mapping at the 595-nm emission, indicating that the defect-related emission only occurs at the thicker CdS microparticle.

relatively thicker CdS rounded microparticle. Those ring-like and size-dependent band edge emissions, as well as strong defect-related emission, provide new possibilities for the construction of optoelectronic devices.

Surface potential and vertical piezoelectricity of CdS thin films

To investigate the surface potential of CdS thin films, SKFM was carried out by noncontact probe scan mode. As shown in Fig. 4A, SKFM can be used to explore the surface potential by tracking the electrostatic interactions between the tip and the sample surface. Such surface potential is related to the work functions of scanned materials and reflects the local charge distribution when a bias voltage was applied to their surface. SKFM has been used to measure the surface potential difference in 2D graphene-boron nitride heterostructures, as well as the doping and charge carrier concentration in semiconducting nanomaterials (*21*, *22*). Figure 4C shows the band diagram change of the AFM tip and sample in SKFM mode. The work function differences between the sample (φ_{sample}) and the probe (φ_{tip}) create a contact potential difference when they are electrically contacted. Therefore,

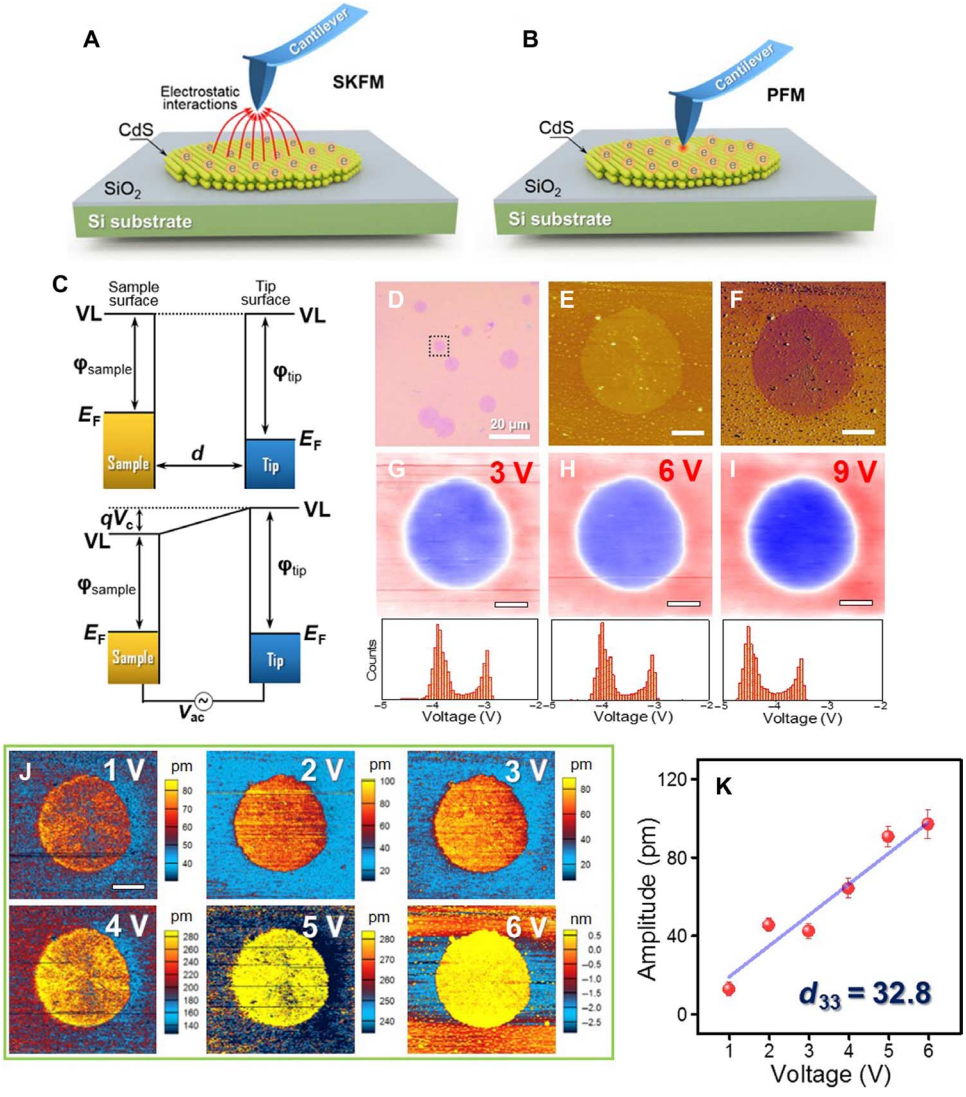

Fig. 4. Noncontact SKFM and standard contact PFM investigation for CdS thin film. (**A** and **B**) Schematic illustration of SKFM (A) and PFM (B) measurements. (**C**) Band diagram of tip and sample when they are electrically separated (top graph) and electrically contacted (bottom graph). *d*, distance; VL, vacuum levels; *q*, electronic charge; V_c, contact potential difference. (**D**) Optical image of CdS thin films. (**E** and **F**) Topography (E) and phase (F) images observed by SKFM mode for the single CdS thin film marked in (D). (**G** to **I**) Corresponding potential mappings with tip voltages of 3, 6, and 9 V, respectively. Insets show histograms of the surface potential distributions. The CdS ultrathin film has a higher positive voltage (~0.9 V) than the substrate, demonstrating that a large amount of charges are accumulated at a CdS thin film after contact PFM scanning. (**J**) Amplitude images observed by contact PFM technology with tip voltages from 1 to 6 V, showing remarkable inverse piezoelectricity. (**K**) Average amplitude variations versus applied voltages calculated from (J). Error bars indicate 1 SD. Scale bars, 2 μm (E to J). The linearly fitted line shows that the measured piezoelectric coefficient d_{eff} is ~16.4 pm·V^{-1}, whereas the vertical piezoelectric coefficient d_{33} is ~32.8 pm·V^{-1}.

tracking the contact potential difference by applying the equivalent external voltage can determine the work function and local charge distribution at the surface of scanned samples. We applied SKFM mode to the single CdS thin films with different tip voltages (3, 6, and 9 V). As seen from the topography and phase images in Fig. 4 (E and F), the CdS thin film presents stronger dark and light contrasts than the substrate. It has a thickness of ~3.09 nm and phase variation of ~3°. Figure 4 (G to I) shows the surface potential images with increased tip voltages, which indicate that the CdS thin film has higher positive voltage than the substrate. The surface potential of CdS sample is quantitatively determined to be ~0.9 V higher than that of the substrate, indicating that a large amount of charges are accumulated at the CdS thin film. We believe that this resulted from the piezoelectricity of the CdS sample because the contact PFM was perfomed several times before the noncontact SKFM measurement. Similar behaviors were also recorded from other CdS samples via SKFM. Before the CdS thin film was scanned by the PFM tip, it showed ~200-mV surface potential, which is higher than the substrate. After scanning, this value increased up to ~1 V (fig. S5). This phenomenon indicates that the contact PFM process can largely change the surface potential of CdS thin film by producing the charges at its surface, and the vertical piezoelectricity of CdS is the key to the generated charges.

We used standard contact PFM technology to investigate the vertical piezoelectricity of single CdS thin film. As shown in Fig. 4B, the mechanical response of the sample was measured when the vertical electrical field was applied to its surface through conducting the PFM tip. A typical piezoelectric material is strained (or stressed) under a vertical electrical field, which is reflected in the amplitude change for PFM imaging. The vertical motion of PFM tip and the vertical electric field applied make PFM imaging a powerful tool to explore the electromechanical functionalities in a vertical direction, namely, quantify the piezoelectric constant of d_{33} for piezoelectric materials. Up to now, this technology has been extensively used to study piezoelectric/ferroelectric ceramic films and ZnO nanomaterials, such as nanowires and nanorods (*23*–*28*), as well as to image domain structures and domain evolution in ferroelectric thin films (*29*–*32*). Here, PFM imaging was first used for local characterization of ultrathin CdS thin films. Tip voltages from 1 to 6 V were applied to study the vertical electromechanical response of CdS thin films. The amplitude images under different tip voltages are shown in Fig. 4J, and the corresponding topography and phase images are displayed in fig. S6. Surprisingly, significant amplitude change was observed in the amplitude images when different tip voltages were applied, indicating strong inverse piezoelectricity. The average amplitude variations can be calculated from the selected areas in Fig. 4J (details in fig. S7). From average amplitude variations versus applied voltages in Fig. 4K, the vertical piezoelectric constant of d_{eff} is ~16.4 pm·V^{-1}, which is not equal to the real vertical piezoelectric coefficient d_{33} because a nonuniform electric field is applied to the sample during the piezoelectric measurements. Pt/Ir-coated tips were used for PFM scanning, and the force applied is in the range of 100 to 200 nN. Such external force will result in a weak indentation to the sample because of the support of the rigid SiO_2 substrate. It is reported that an AFM tip can only penetrate ~3 nm at SiO_2 (*3*). The thin and soft nature of the CdS (~3 nm) ensures that the mechanical deformation of SiO_2 is the dominant contribution, as shown in fig. S8. The stiff tip and surface and high dielectric constant lead to a significant potential drop between the tip and surface, that is, $V_s \ll V_{tip}$, and the contact area is negligible in this situation (*33*). The nonplanar PFM tip and small deformation of rigid substrate result in a weak indentation limit and make the contact area with the sample less than the tip radius (~25 nm) (fig. S8). According to previous reports (*32*–*34*), the value of d_{33} is approximately twice than measured d_{eff}. On this basis, we can estimate the piezoelectric coefficient d_{33} of the CdS thin film to be 32.8 pm·V^{-1}, which is three times larger than that of the bulk CdS materials (9.71 pm·V^{-1}) and ZnO materials, and even comparable to some of the inorganic piezoelectric ceramics (see fig. S9 and table S1) (*35*). Previous studies have demonstrated that the piezoelectric coefficient of CdS strongly depended on its carrier concentration. The d_{33} coefficient of CdS decreased by 60% when the carrier concentration increased from 10^9 to 10^{18} cm^{-3} (*36*, *37*). To investigate the electrical conductivity of CdS materials, we fabricated the Hall device and field-effect transistor devices (figs. S10 and S11). The Hall device presents poor conductivity, and picoampere-level current can be detected under higher source-drain voltage, making it difficult for the Hall device to calculate the carrier concentration. We further fabricated the field-effect transistor using the single CdS thin film (see fig. S11). The source-drain current was measured at the picoampere level when a bias voltage (25 V) was applied, indicating the low carrier concentration in our CdS thin film. The carrier concentration (n_c) can be calculated by $n_c = 1/\rho e\mu_e$, where ρ is the resistivity, e is the electronic charge, and μ_e is the electron mobility (*36*). Electron mobility (μ_e) can be estimated by $\mu_e = G_m(L/WC_gV_{ds})$, where G_m is the peak transconductance ($G = dI_{ds}/dV_g$), C_g is the gate capacitance, and L and W are the channel length (7 μm) and width (10 μm), respectively. We deduce that the mobility μ_e is 0.0023 cm^2 V^{-1} s^{-1}, and the carrier concentration n_c is in the range of ~10^{12} to ~10^{15} cm^{-3}. Therefore, this robust piezoelectric coefficient of CdS thin film is presumably due to the free boundary and low carrier concentration, which results from the low dimensional structure with large surface and defects.

DART-PFM technology for imaging vertical piezoelectric domain

The DART-PFM was used to understand the piezoelectricity of CdS thin films by in-site characterization. Although PFM technology is considered to be a powerful tool to monitor the electromechanical response of piezoelectric materials, it fails at rough surface or atomic thin films. For such samples, the noise floors of the surface height topography usually reach tens of picometers, which is comparable to the electromechanical displacement in atomically thin nanomaterials at the vertical direction. As shown in fig. S12, DART-PFM uses dual ac resonance tracking to measure the shift of resonance frequency while avoiding crosstalk between changes in the contact resonance frequency and surface topography (*38*, *39*). DART-PFM has proven to be a reliable method to study the electromechanical elastic properties of inorganic ceramics and biological systems (*38*). Here, we used this technology to investigate the local piezoelectricity of CdS thin films (Fig. 5, A to K). Figure 5A shows the height topography of single CdS thin film with a thickness of ~3.16 nm. The corresponding resonant frequency, phase, and amplitude images are displayed in Fig. 5 (B to D). For the resonant frequency image, the CdS thin film (dark) shows a remarkable contrast against the regions outside (bright) because the resonant frequency of the tip-surface interaction changes from ~347 to 342 kHz when the tip is applied to the CdS thin film. The corresponding phase change is also observed, as shown in Fig. 5C. This variation of resonant frequency probably results from the tip-surface spring constant, which originated

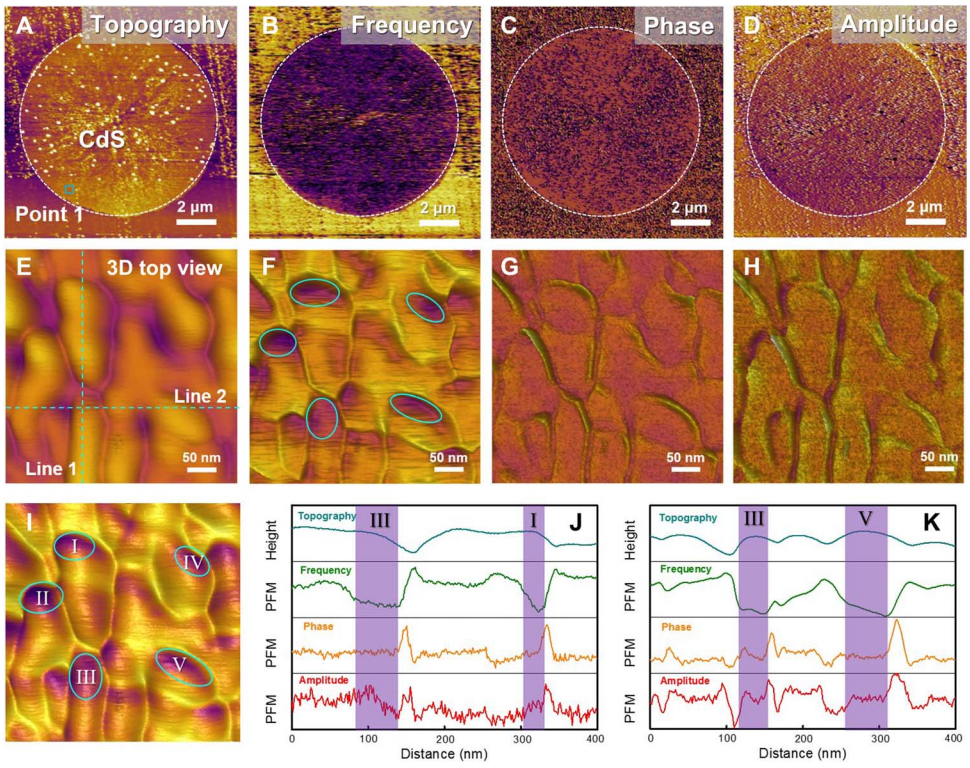

Fig. 5. DART-PFM technology for characterization of CdS thin film. (**A** to **D**) Topography (A), resonance frequency (B), phase (C), and amplitude (D) images for a single CdS thin film, showing remarkable resonance frequency variations. (**E** to **H**) Top-view 3D topography (E), resonance frequency (F), phase (G), and amplitude (H) images for marked area in (A). (**I**) Overlap image of topography and resonance frequency. Marked areas present the notable change of resonance frequency. (**J** and **K**) Height profiles measured by line scans along lines 1 and 2 in (E), and shadow areas (I, III, and V) corresponding to marked areas in (I).

from the electromechanical reaction and piezoelectric constant of the materials being scanned. To understand the vertical piezoelectric of the surface of CdS thin film locally, the imaging area was zoomed to 400 × 400 nm, as marked in Fig. 5A. The top view of 3D topography, resonance frequency, phase, and amplitude images are shown in Fig. 5 (E to H, respectively). The height topography shows that the CdS thin film is composed of ultrathin nanosheets (roughness, 0.67 nm). The resonance frequency of a small nanosheet varies from ~346 to ~343 kHz at different locations (Fig. 5F). The contrast is observed from the marked areas (I, II, III, IV, and V) in the overlap images of topography and frequency in Fig. 5I and the corresponding height profiles in Fig. 5 (J and K). The dark areas represent low resonance frequency, implying the strong piezoelectric domains. Similar piezoelectric geometries were also found at the boundary between the CdS thin film and substrate, as shown in fig. S13. As mentioned above, the frequency response in such scanning model is dominated by the tip-sample electromechanical interaction, which mainly relies on the piezoelectricity and the crystallinity of samples. Therefore, it enables us to study the electromechanical properties locally on the rough surface of the atomic nanosheets.

Simulation on vertical piezoelectricity and actuator with subatomic resolution

To better explain the experimental results of vertical piezoelectricity and estimate the deformation of CdS thin film under applied voltage, we developed a 3D finite element (FE) model with COMSOL Multiphysics, as schematically shown in Fig. 6. This model consists of a cone with a half ball as the PFM tip, which has a diameter of 50 nm (Fig. 6A), and one CdS sample with a thickness of 3 nm. In this simulation setup, the PFM tip contacts the CdS sample, to which a 5-V dc voltage was applied. The stress distributions on the CdS sample were investigated, as shown in Fig. 6 (C and D). The region surrounding the contact point experiences the highest stress. The stress then decays gradually toward the edges of the CdS sample. The strong stress is contributed by the large deformation produced by vertical piezoelectricity of the CdS sample. This unprecedented high vertical piezoelectricity (d_{33} = 32.8 pm·V^{-1}) of CdS thin film allows extremely precise positioning at the subatomic level. We built a 3D FE model to demonstrate this. CdS thin film (thickness of 3 nm and radius of 15 nm) was used as the actuating material, and −1- to −5-V dc voltages were applied to its surface as driven voltages. Applying a negative tip bias to the CdS surface leads to a positive electrical field along the vertical direction and results in the expansion of materials. Figure 6 (E to G) shows the simulation results of a strained CdS thin film with different voltages applied to its surface. By increasing the negative driven voltage from −1 to −5 V, the deformation of the CdS sample was linearly increased from ~30 to ~150 pm (Fig. 6, E and F). This result is in accordance with experimental data. Although the roughness of the CdS thin film is increased slightly under large potential (Fig. 6E), the deformation magnitude remains linearly dependent on the driven voltage at the picometer level, which is already close to the lattice constant of CdS. Our simulation demonstrates high vertical piezoelectricity in CdS thin film, which can be applied as an active material for subatomic deformation actuators.

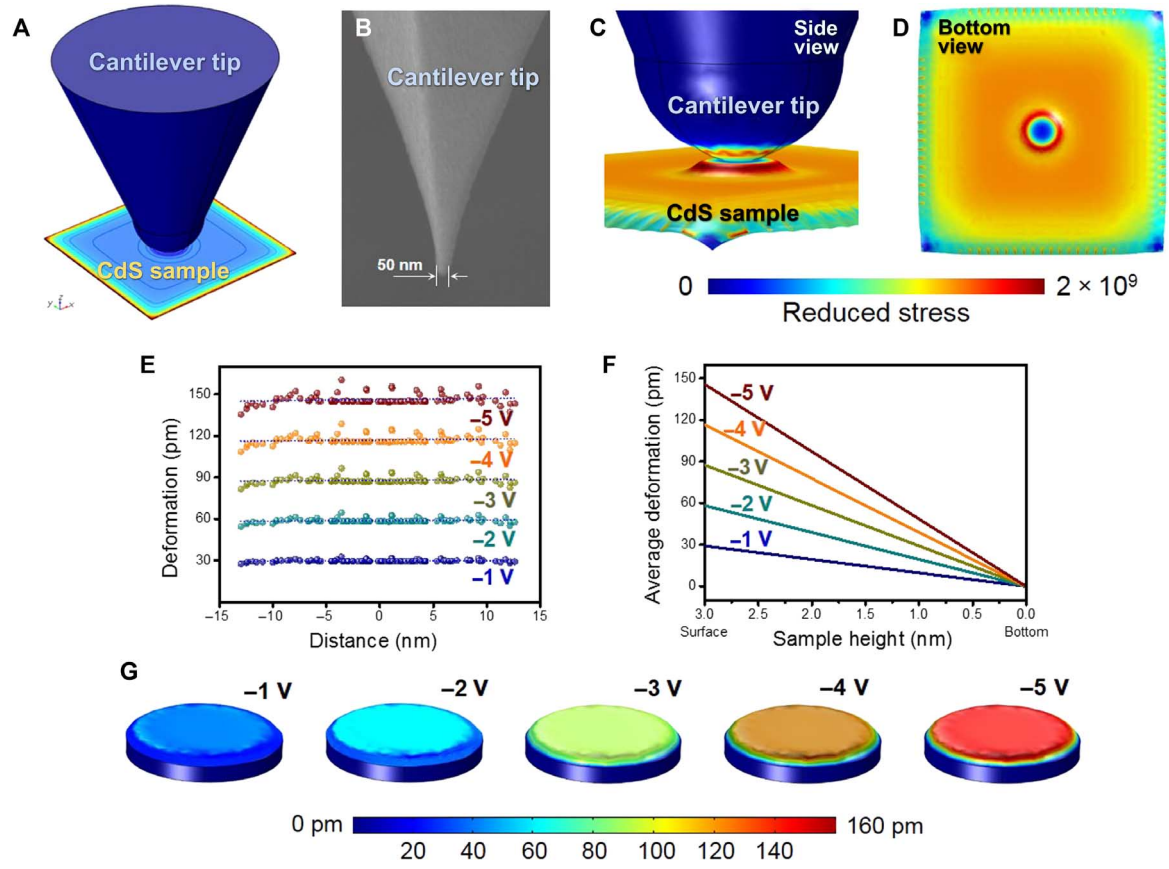

Fig. 6. Simulation of vertical piezoelectricity and subatomic deformation actuator. (**A**) Three-dimensional image of potential drop on CdS film. (**B**) Scanning electron microscopy image of a conductive tip for PFM characterization. (**C** and **D**) Bottom and side views of stress distribution on CdS film. (**E** to **G**) Simulation for subatomic deformation actuator. Different potentials were applied to surface deformation curves (E), mappings (G), and vertical deformation (F) of CdS thin films.

CONCLUSIONS

In summary, we prepared ultrathin CdS thin films and demonstrated their strong vertical piezoelectricity at the atomic scale (three to five space lattices) by using noncontact SKFM, contact PFM, and DART-PFM. We resolved the locally vertical piezoelectricity of CdS thin films using DART-PFM and determined the vertical piezoelectric domains at the CdS thin films. Their vertical piezoelectric coefficient (d_{33}) was ~32.8 pm·V^{-1}, which was three times higher than the CdS bulk. In addition, vertical piezoelectricity in the CdS thin film and its applications in subatomic deformation actuators were demonstrated by 3D FE models. Strong vertical piezoelectricity makes this material promising for the construction of atomically thin piezoelectric devices.

MATERIALS AND METHODS

Growth of CdS thin films

The synthesis of ultrathin CdS nanoplatelets was carried out in a conventional tube furnace (ThermoFisher, Lindberg/Blue MTF55035C-1) equipped with a 1-inch quartz tube and connected to Ar gas inlets (fig. S1). The starting materials were sulfur (1 g) and Cd grain (60 mg), which were placed in different porcelain boats inside the quartz tube. The Si/SiO_2 substrates (230-nm SiO_2 on Si) were placed downstream of the Cd grain and at the center of the furnace to collect the products. Then, the system was flushed with argon flow (100 sccm) for more than three cycles and heated to the targeted temperature of 600°C, with a rate of 20°C/min. When the temperature reached and kept in targeted temperature for 30 min, the furnace was instantly switched off and cooled down to room temperature naturally. Finally, the CdS thin films were grown on the Si/SiO_2 substrate.

Characterization and 3D FE simulation

Both Raman and PL data were collected at room temperature using 457-nm laser as an excitation source (WITec alpha300 RAS Raman system). Sample size, thickness, morphologies, surface potential, and vertical piezoelectricity were evaluated with optical microscopy (Olympus BX51), AFM, SKFM, PFM, and DART-PFM (Cypher S, Asylum Research). The FE simulation of the vertical piezoelectricity and subatomic deformation actuator was performed with FE modeling software (COMSOL Multiphysics 5.0). Details can be found in the Supplementary Materials.

SUPPLEMENTARY MATERIALS

Supplementary material for this article is available at http://advances.sciencemag.org/cgi/content/full/2/7/e1600209/DC1

Supplementary Materials and Methods
fig. S1. Growth of CdS thin films.
fig. S2. Statistical analysis for the size of CdS thin films.
fig. S3. Raman spectra of as-obtained CdS sample.
fig. S4. PL spectra and PL mapping from the CdS thin films.
fig. S5. SKFM characterization of CdS thin film.
fig. S6. Topography and phase images of PFM characterization of CdS thin film when different tip voltages (1 to 6 V) were applied.
fig. S7. The average amplitude change can be established from eight different areas of CdS sample.
fig. S8. Illustration of weak indentation and strong indentation.
fig. S9. Thickness versus piezoelectric coefficient distribution from previous literature results.
fig. S10. Hall device of CdS thin film.
fig. S11. Electrical characterization of CdS thin film.
fig. S12. Schematic illustration of experimental setup for DART-PFM.
fig. S13. DART-PFM characterization for the boundary of CdS thin film.
table S1. Summary of piezoelectric coefficient from different materials.
References (*40*–*50*)

REFERENCES AND NOTES

1. H. Zhu, Y. Wang, J. Xiao, M. Liu, S. Xiong, Z. J. Wong, Z. Ye, Y. Ye, X. Yin, X. Zhang, Observation of piezoelectricity in free-standing monolayer MoS_2. *Nat. Nanotechnol.* **10**, 151–155 (2015).
2. W. Wu, L. Wang, Y. Li, F. Zhang, L. Lin, S. Niu, D. Chenet, X. Zhang, Y. Hao, T. F. Heinz, J. Hone, Z. L. Wang, Piezoelectricity of single-atomic-layer MoS_2 for energy conversion and piezotronics. *Nature* **514**, 470–474 (2014).
3. J. Qi, Y.-W. Lan, A. Z. Stieg, J.-H. Chen, Y.-L. Zhong, L.-J. Li, C.-D. Chen, Y. Zhang, K. L. Wang, Piezoelectric effect in chemical vapour deposition-grown atomic-monolayer triangular molybdenum disulfide piezotronics. *Nat. Commun.* **6**, 7430 (2015).
4. K.-A. N. Duerloo, M. T. Ong, E. J. Reed, Intrinsic piezoelectricity in two-dimensional materials. *J. Phys. Chem. Lett.* **3**, 2871–2876 (2012).
5. M. Zelisko, Y. Hanlumyuang, S. Yang, Y. Liu, C. Lei, J. Li, P. M. Ajayan, P. Sharma, Anomalous piezoelectricity in two-dimensional graphene nitride nanosheets. *Nat. Commun.* **5**, 4284 (2014).
6. S. Manzeli, A. Allain, A. Ghadimi, A. Kis, Piezoresistivity and strain-induced band gap tuning in atomically thin MoS_2. *Nano Lett.* **15**, 5330–5335 (2015).
7. S. Ithurria, M. D. Tessier, B. Mahler, R. P. S. M. Lobo, B. Dubertret, A. L. Efros, Colloidal nanoplatelets with two-dimensional electronic structure. *Nat. Mater.* **10**, 936–941 (2011).
8. X.-D. Wen, R. Hoffmann, N. W. Ashcroft, Two-dimensional CdSe nanosheets and their interaction with stabilizing ligands. *Adv. Mater.* **25**, 261–266 (2013).
9. C. Bouet, B. Mahler, B. Nadal, B. Abecassis, M. D. Tessier, S. Ithurria, X. Xu, B. Dubertret, Two-dimensional growth of CdSe nanocrystals, from nanoplatelets to nanosheets. *Chem. Mater.* **25**, 639–645 (2013).
10. S. Pedetti, S. Ithurria, H. Heuclin, G. Patriarche, B. Dubertret, Type-II CdSe/CdTe core/crown semiconductor nanoplatelets. *J. Am. Chem. Soc.* **136**, 16430–16438 (2014).
11. V. Sivasubramanian, A. K. Arora, M. Premila, C. S. Sundar, V. S. Sastry, Optical properties of CdS nanoparticles upon annealing. *Physica E* **31**, 93–98 (2006).
12. C. Hu, X. Zeng, J. Cui, H. Chen, J. Lu, Size effects of Raman and photoluminescence spectra of CdS nanobelts. *J. Phys. Chem. C* **117**, 20998–21005 (2013).
13. H. M. Fan, Z. H. Ni, Y. P. Feng, X. F. Fan, J. L. Kuo, Z. X. Shen, B. S. Zou, Anisotropy of electron–phonon coupling in single wurtzite CdS nanowires. *Appl. Phys. Lett.* **91**, 171911 (2007).
14. S. Kar, B. Satpati, P. V. Satyam, S. Chaudhuri, Synthesis and optical properties of CdS nanoribbons. *J. Phys. Chem. B* **109**, 19134–19138 (2005).
15. A. P. Alivisatos, Semiconductor clusters, nanocrystals, and quantum dots. *Science* **271**, 933–937 (1996).
16. J. Tian, G. Cao, Semiconductor quantum dot-sensitized solar cells. *Nano Rev.* **4**, 10.3402/nano.v4i0.22578 (2013).
17. B. B. Srivastava, S. Jana, N. Pradhan, Doping Cu in semiconductor nanocrystals: Some old and some new physical insights. *J. Am. Chem. Soc.* **133**, 1007–1015 (2011).
18. N. N. Hewa-Kasakarage, M. Kirsanova, A. Nemchinov, N. Schmall, P. Z. El-Khoury, A. N. Tarnovsky, M. Zamkov, Radiative recombination of spatially extended excitons in (ZnSe/CdS)/CdS heterostructured nanorods. *J. Am. Chem. Soc.* **131**, 1328–1334 (2009).
19. R. Banerjee, R. Jayakrishnan, R. Banerjee, P. Ayyub, Effect of the size-induced structural transformation on the band gap in CdS nanoparticles. *J. Phys. Condens. Matter* **12**, 10647–10654 (2000).
20. D. A. B. Miller, D. S. Chemla, T. C. Damen, A. C. Gossard, W. Wiegmann, T. H. Wood, C. A. Burrus, Band-edge electroabsorption in quantum well structures: The quantum-confined Stark effect. *Phys. Rev. Lett.* **53**, 2173–2176 (1984).
21. T. Gao, X. Song, H. Du, Y. Nie, Y. Chen, Q. Ji, J. Sun, Y. Yang, Y. Zhang, Z. Liu, Temperature-triggered chemical switching growth of in-plane and vertically stacked graphene-boron nitride heterostructures. *Nat. Commun.* **6**, 6835 (2015).
22. C. Maragliano, S. Lilliu, M. S. Dahlem, M. Chiesa, T. Souier, M. Stefancich, Quantifying charge carrier concentration in ZnO thin films by Scanning Kelvin Probe Microscopy. *Sci. Rep.* **4**, 4203 (2014).
23. E. Broitman, M. Y. Soomro, J. Lu, M. Willander, L. Hultman, Nanoscale piezoelectric response of ZnO nanowires measured using a nanoindentation technique. *Phys. Chem. Chem. Phys.* **15**, 11113–11118 (2013).
24. Y.-F. Lin, J. Song, Y. Ding, S.-Y. Lu, Z. L. Wang, Piezoelectric nanogenerator using CdS nanowires. *Appl. Phys. Lett.* **92**, 022105 (2008).
25. C. Harnagea, M. Alexe, D. Hesse, A. Pignolet, Contact resonances in voltage-modulated force microscopy. *Appl. Phys. Lett.* **83**, 338 (2003).
26. N. V. Andreeva, M. Tyunia, A. V. Filimonov, A. I. Rudskoy, N. A. Pertsev, S. B. Vakhrushev, Low-temperature evolution of local polarization properties of $PbZr_{0.65}Ti_{0.35}O_3$ thin films probed by piezoresponse force microscopy. *Appl. Phys. Lett.* **104**, 112905 (2014).
27. L. Aggarwal, J. S. Sekhon, S. N. Guin, A. Arora, D. S. Negi, R. Datta, K. Biswas, G. Sheet, Direct evidence of strong local ferroelectric ordering in a thermoelectric semiconductor. *Appl. Phys. Lett.* **105**, 113903 (2014).
28. M. Hussain, A. Khan, O. Nur, M. Willander, E. Broitman, The effect of oxygen-plasma treatment on the mechanical and piezoelectrical properties of ZnO nanorods. *Chem. Phys. Lett.* **608**, 235–238 (2014).
29. M. Trapatseli, D. Carta, A. Regoutz, A. Khiat, A. Serb, I. Gupta, T. Prodromakis, Conductive atomic force microscopy investigation of switching thresholds in titanium dioxide thin films. *J. Phys. Chem. C* **119**, 11958–11964 (2015).
30. C. Li, L. Huang, T. Li, W. Lü, X. Qiu, Z. Huang, Z. Liu, S. Zeng, R. Guo, Y. Zhao, K. Zeng, M. Coey, J. Chen, Ariando, T. Venkatesan, Ultrathin $BaTiO_3$-based ferroelectric tunnel junctions through interface engineering. *Nano Lett.* **15**, 2568–2573 (2015).
31. A. Belianinov, Q. He, A. Dziaugys, P. Maksymovych, E. Eliseev, A. Borisevich, A. Morozovska, J. Banys, Y. Vysochanskii, S. V. Kalinin, $CuInP_2S_6$ room temperature layered ferroelectric. *Nano Lett.* **15**, 3808–3814 (2015).
32. B. Y. Lee, J. Zhang, C. Zueger, W.-J. Chung, S. Y. Yoo, E. Wang, J. Meyer, R. Ramesh, S.-W. Lee, Virus-based piezoelectric energy generation. *Nat. Nanotechnol.* **7**, 351–356 (2012).
33. S. V. Kalinin, D. A. Bonnell, Imaging mechanism of piezoresponse force microscopy of ferroelectric surfaces. *Phys. Rev. B* **65**, 125408 (2002).
34. F. Johann, Á. Hoffmann, E. Soergel, Impact of electrostatic forces in contact-mode scanning force microscopy. *Phys. Rev. B* **81**, 094109 (2010).
35. H. D. Espinosa, R. A. Bernal, M. Minary-Jolandan, A review of mechanical and electromechanical properties of piezoelectric nanowires. *Adv. Mater.* **24**, 4656–4675 (2012).
36. D. A. Scrymgeour, J. W. P. Hsu, Correlated piezoelectric and electrical properties in individual ZnO nanorods. *Nano Lett.* **8**, 2204–2209 (2008).
37. T. Ogawa, H. Oikawa, A. Kojima, Decrement caused by screening effect of conduction electrons on the effective charge of CdS crystals. *Jap. J. Appl. Phys.* **10**, 593–599 (1971).
38. B. J. Rodriguez, C. Callahan, S. V. Kalinin, R. Proksch, Dual-frequency resonance-tracking atomic force microscopy. *Nanotechnology* **18**, 475504 (2007).
39. A. Gannepalli, D. G. Yablon, A. H. Tsou, R. Proksch, Mapping nanoscale elasticity and dissipation using dual frequency contact resonance AFM. *Nanotechnology* **22**, 355705 (2011).
40. D. F. Crisler, J. J. Cupal, A. R. Moore, Dielectric, piezoelectric, and electromechanical coupling constants of zinc oxide crystals, *Proc. IEEE* **56**, 225–226 (1968).
41. D. A. Scrymgeour, T. L. Sounart, N. C. Sinnons, J. W. P. Hsu, Polarity and piezoelectric response of solution grown zinc oxide nanocrystals on silver. *J. Appl. Phys.* **101**, 014316 (2007).
42. M.-H. Zhao, Z.-L. Wang, S. X. Mao, Piezoelectric characterization of individual zinc oxide nanobelt probed by piezoresponse force microscope. *Nano Lett.* **4**, 587–590 (2004).
43. H. J. Fan, W. Lee, R. Hauschild, M. Alexe, G. Le Rhun, R. Scholz, A. Dadgar, K. Nielsch, H. Kalt, A. Krost, M. Zacharias, U. Gösele, Template-assisted large-scale ordered arrays of ZnO pillars for optical and piezoelectric applications. *Small* **2**, 561–568 (2006).
44. T.-Y. Ke, H.-A. Chen, H.-S. Sheu, J.-W. Yeh, H.-N. Lin, C.-Y. Lee, H.-T. Chiu, Sodium niobate nanowire and its piezoelectricity. *J. Phys. Chem. C* **112**, 8827–8831 (2008).
45. J. Wang, C. Stampfer, C. Roman, W. H. Ma, N. Setter, C. Hierold, Piezoresponse force microscopy on doubly clamped $KNbO_3$ nanowires. *Appl. Phys. Lett.* **93**, 223101 (2008).
46. Z. Wang, A. P. Suryavanshi, M.-F. Yu, Ferroelectric and piezoelectric behaviors of individual single crystalline $BaTiO_3$ nanowire under direct axial electric biasing. *Appl. Phys. Lett.* **89**, 082903 (2006).
47. M. Minary-Jolandan, R. A. Bernal, I. Kuljanishvili, V. Parpoil, H. D. Espinosa, Individual GaN nanowires exhibit strong piezoelectricity in 3D. *Nano Lett.* **12**, 970–976 (2012).
48. Y. Luo, I. Szafraniak, N. D. Zakharov, V. Nagarajan, M. Steinhart, R. B. Wehrspohn, J. H. Wendorff, R. Ramesh, M. Alexe, Nanoshell tubes of ferroelectric lead zirconate titanate and barium titanate. *Appl. Phys. Lett.* **83**, 440 (2003).
49. T. D. Nguyen, J. M. Nagarah, Y. Qi, S. S. Nonnenmann, A. V. Morozov, S. Li, C. B. Arnold, M. C. McAlpine, Wafer-scale nanopatterning and translation into high-performance piezoelectric nanowires. *Nano Lett.* **10**, 4595–4599 (2010).

50. R. Blachnik, J. Chu, R. R. Galązka, J. Geurts, J. Gutowski, B. Hönerlage, D. Hofmann, J. Kossut, R. Lévy, P. Michler, U. Neukirch, D. Strauch, T. Story, A. Waag, II-VI and I-VII compounds; semimagnetic compounds, in *Landolt-Börnstein: Numerical Data and Functional Relationships in Science and Technology*, O. Madelung, U. Rossler, M. Schulz, Eds. (Springer, Berlin, 1999) vol. 41B.

Acknowledgments

Funding: This work is supported by the Singapore National Research Foundation (NRF) (NRF RF Award No. NRF-RF2013-08), National Program on Key Basic Research Project (973 Program, Grand No. 2015CB351901), the National Natural Science Foundation of China (61574163), and a start-up funding from Nanyang Technological University (M4081137.070). **Author contributions:** Z.L., T.Z., and Xuewen Wang conceived and designed the experiments; Xuewen Wang and X.H. performed the growth of materials and SKFM and PFM characterizations. L.S. and Xingli Wang conducted Raman and PL measurements. Xuewen Wang and L.C.H. carried out the DART-PFM measurement. H.Z. performed finite element analysis simulation. Xuewen Wang, Z.L., and T.Z. cowrote the paper. All authors contributed to the result analysis and discussions. **Competing interests:** Z.L. and Xuewen Wang are inventors of the technology which is patent pending (Application 10201604725P). **Data and materials availability:** All data needed to evaluate the conclusions in the paper are present in the paper and/or the Supplementary Materials. Additional data related to this paper may be requested from the authors.

Submitted 2 February 2016
Accepted 12 May 2016
Published 1 July 2016
10.1126/sciadv.1600209

Citation: X. Wang, X. He, H. Zhu, L. Sun, W. Fu, X. Wang, L. C. Hoong, H. Wang, Q. Zeng, W. Zhao, J. Wei, Z. Jin, Z. Shen, J. Liu, T. Zhang, Z. Liu, Subatomic deformation driven by vertical piezoelectricity from CdS ultrathin films. *Sci. Adv.* **2**, e1600209 (2016).

Science Advances

Subatomic deformation driven by vertical piezoelectricity from CdS ultrathin films

Xuewen Wang, Xuexia He, Hongfei Zhu, Linfeng Sun, Wei Fu, Xingli Wang, Lai Chee Hoong, Hong Wang, Qingsheng Zeng, Wu Zhao, Jun Wei, Zhong Jin, Zexiang Shen, Jie Liu, Ting Zhang and Zheng Liu

Sci Adv **2** (7), e1600209.
DOI: 10.1126/sciadv.1600209